Retinal Neuroprotective Effect of Mesenchymal Stem Cells Secretome Through Modulation of Oxidative Stress, Autophagy, and Programmed Cell Death

Ricardo Usategui-Martín,[1–4] Kevin Puertas-Neyra,[1] Nadia Galindo-Cabello,[1,5] Leticia A. Hernández-Rodríguez,[1] Fernando González-Pérez,[6] José Carlos Rodríguez-Cabello,[2,6] Rogelio González-Sarmiento,[7–9] José Carlos Pastor,[1–4] and Ivan Fernandez-Bueno[1–4]

[1]Instituto Universitario de Oftalmobiología Aplicada, Retina Group, Universidad de Valladolid, Valladolid, Spain
[2]Centro en Red de Medicina Regenerativa y Terapia Celular de Castilla y León, Valladolid, Spain
[3]Red Temática de Investigación Cooperativa en Salud, Oftared, Instituto de Salud Carlos III, Valladolid, Spain
[4]RetiBrain (RED2018-102499-T), Ministerio de Ciencia, Innovación y Universidades, Valladolid, Spain
[5]Postgraduate Unit, Faculty of Biological Sciences, National University of San Marcos, Lima, Peru
[6]Group for Advanced Materials and Nanobiotechnology (GIR BIOFORGE), CIBER-BBN, Edificio LUCIA, Universidad de Valladolid, Paseo Belén 19, Valladolid, Spain
[7]Molecular Medicine Unit, Department of Medicine, University of Salamanca, Salamanca, Spain
[8]Institute of Biomedical Research of Salamanca, Salamanca, Spain
[9]Institute of Molecular and Cellular Biology of Cancer, University of Salamanca-CSIC, Salamanca, Spain

Correspondence: Ivan Fernandez-Bueno, Instituto Universitario de Oftalmobiología Aplicada, Universidad de Valladolid, Campus Miguel Delibes, Paseo de Belén 17, 47011 Valladolid, Spain; ifernandezb@ioba.med.uva.es.
Ricardo Usategui-Martín, Instituto Universitario de Oftalmobiología Aplicada, Universidad de Valladolid, Campus Miguel Delibes, Paseo de Belén 17, 47011 Valladolid, Spain; rusateguim@ioba.med.uva.es.

Received: October 18, 2021
Accepted: April 2, 2022
Published: April 29, 2022

Citation: Usategui-Martín R, Puertas-Neyra K, Galindo-Cabello N, et al. Retinal neuroprotective effect of mesenchymal stem cells secretome through modulation of oxidative stress, autophagy, and programmed cell death. *Invest Ophthalmol Vis Sci.* 2022;63(4):27. https://doi.org/10.1167/iovs.63.4.27

Purpose. Degenerative mechanisms of retinal neurodegenerative diseases (RND) share common cellular and molecular signalization pathways. Curative treatment does not exist and cell-based therapy, through the paracrine properties of mesenchymal stem cells (MSC), is a potential unspecific treatment for RND. This study aimed to evaluate the neuroprotective capability of human bone marrow (bm) MSC secretome and its potential to modulate retinal responses to neurodegeneration.

Methods. An in vitro model of spontaneous retinal neurodegeneration was used to compare three days of monocultured neuroretina (NR), NR cocultured with bmMSC, and NR cultured with bmMSC secretome. We evaluated retinal morphology markers (Lectin peanut agglutinin, rhodopsin, protein kinase C α isoform, neuronal-specific nuclear protein, glial fibrillary acidic protein, TdT-mediated dUTP nick-end labeling, and vimentin) and proteins involved in apoptosis (apoptosis-inductor factor, caspase-3), necroptosis (MLKL), and autophagy (p62). Besides, we analyzed the relative mRNA expression through qPCR of genes involved in apoptosis (*BAX, BCL2, CASP3, CASP8, CASP9*), necroptosis (*MLKL, RIPK1, RIPK3*), autophagy (*ATG7, BCLIN1, LC3B, mTOR, SQSTM1*), oxidative stress (*COX2, CYBA, CYBB, GPX6, SOD1, TXN2, TXNRD1*) and inflammation (*IL1, IL6, IL10, TGFb1, TNFa*).

Results. The bmMSC secretome preserves retinal morphology, limits pro-apoptotic– and pro-necroptotic–related gene and protein expression, modulates autophagy-related genes and proteins, and stimulates the activation of antioxidant-associated genes.

Conclusions. The neuroprotective ability of the bmMSC secretome is associated with activation of antioxidant machinery, modulation of autophagy, and inhibition of apoptosis and necroptosis during retinal degeneration. The neuroprotective effect of bmMSC secretomes in the presence/absence of MSC looks similar. Our current results reinforce the hypothesis that the human bmMSC secretome slows retinal neurodegeneration and may be a therapeutic option for treating RND.

Keywords: retina, cell therapy, neurodegeneration, neuroprotection, oxidative stress, programmed cell death

Retinal neurodegenerative diseases (RND), including age-related macular degeneration, glaucoma, diabetic retinopathy, retinitis pigmentosa, and others, are the most common cause of irreversible low vision and blindness. Population-based studies have reported that the prevalence rates of retinal neurodegenerative disorders range from 5.35% to 21.02% in people over age 40 years.[1–3] RND causes progressive visual loss with dramatic clinical, social, and

iovs.arvojournals.org | ISSN: 1552-5783

economic consequences that significantly impact patient quality of life.[4] Retinal neurodegeneration is triggered by different causes, including genetic alterations, intraocular pressure variations, metabolic diseases such as diabetes, or other types of stress or aging.[5] Although the etiology and clinical characteristics of retinal RND can differ phenotypically, the neurodegenerative processes of these diseases are similar because of common cellular and molecular responses.[1,5] Thus an inflammatory response, oxidative stress, reactive gliosis, and activation of cellular death and autophagy pathways are typical in retinal RND.[5,6]

Currently, there is no curative treatment for RND, and available therapies cannot even slow the progression of visual loss in some RND.[5] However, the sequence of pathophysiological events in RND is closely related, making them an appropriate target for unspecific therapies such as cell-based therapy. The cell therapy mostly applied for RND used mesenchymal stem cells (MSC),[7,8] which are the principal approach to neuroprotection through the paracrine properties of the MSC due to its low integration rate in the retinal tissue.[9] Several proteins secreted by MSC are neuroprotective against retinal degeneration by promoting overall cellular homeostasis and preserving cell viability.[5,10–12] In this scenario, developing a cell-free therapeutic strategy based on the production of "MSC secretome cocktails" with neuroprotective characteristics may be a promising therapeutic strategy for treating RND.[13,14] This strategy also may have substantial advantages over therapy based on living cells.[13]

This study aimed to evaluate the potential neuroprotective effect of human bmMSC secretome in an in vitro porcine model of spontaneous retinal neurodegeneration and studied how the bmMSC secretome modulates the cellular and molecular neuroretinal (NR) response to the neurodegenerative process.

Materials and Methods

Human bmMSC Culture Conditions

According to the International Society for Cell Therapy, human bmMSC derived from two healthy women of 51 and 54 years old were supplied by Citospin S.L. (Valladolid, Spain) after characterization. Briefly, the bmMSC were positive for the MSC antigens (CD105, CD90, CD73, and CD166) and negative for specific markers of hematopoietic cells (CD14, CD34, CD45, and HLA-DR). Human bmMSC were produced under good manufacturing standards. The Spanish Drug Agency previously approved human bmMSCs from Citospin S.L. in clinical trials (European Union Drug Regulating Authorities Clinical Trials Database) (clinicaltrials.gov identifiers: 2011-005321-51 [NCT01586312] and 2016-003029-40 [NCT03173638]). Furthermore, our group has previously used the human bmMSC from Citospin S.L. in both in vivo and in vitro experiments.[11,12,15]

Cell viability and cell counts were determined using a trypan blue assay (Sigma-Aldrich, St. Louis, MO, USA) and a TC20 automated cell counter (Bio-Rad, Hercules, CA, USA). The bmMSC were seeded on the bottoms of Transwell 24-mm-diameter culture plates (Corning Life Sciences, Corning, NY) in Dulbecco's modified Eagle medium (DMEM) supplemented with 10% fetal bovine serum (FBS) (Gibco, Invitrogen, Carlsbad, CA, USA), 1% antibiotics (100 U/mL penicillin and 100 mg/mL streptomycin) (Gibco, Invitrogen), and 1% L-glutamine (Sigma-Aldrich); 30,000 cells/well of human bmMSCs were seeded. The bmMSC were cultured at 37°C in a 5% CO_2 atmosphere for 72 hours until confluence for subsequent co-culturing with NR explants.

Central NR Explant Preparation and Culture Conditions

Fresh eyes (n = 8) were obtained from pigs aged 6 to 8 months from a local slaughterhouse. The NR explants were obtained less than 2 hours after enucleation, as described.[16] Four adjacent NR explants from the *area centralis* (i.e., the cone-enriched visual streak without blood vessels) were obtained from each eye (n = 32). The explants were laid on Transwell membranes 24 mm in diameter with a 0.4-mm-pore polycarbonate membrane insert (Corning Life Sciences) with the photoreceptor layer facing the membrane.

Explants were mono-cultured or co-cultured with bmMSC in the same culture well and physically separated by the Transwell porous membrane that prevented migration of the bmMSC and integration into the NR tissue.[17] We maintained cultures in 1.5 mL of DMEM/Neurobasal-A (1:1) medium supplemented with 10% FBS, 1% antibiotics, 2% B-27, and 1% L-glutamine (Gibco, Invitrogen). The third condition was culturing the NR explants with 0.75 mL of medium from the co-culture of the explants with bmMSC and 0.75 mL of DMEM/Neurobasal-A (1:1) medium supplemented with 10% FBS, 1% antibiotics, 2% B-27, and 1% L-glutamine. All cultures were maintained under standard conditions (37°C in a 5% CO_2 atmosphere) for 72 hours. The NR explants were obtained and processed in parallel before culturing (fresh NR explants).

Four experimental conditions were analyzed: fresh neuroretinas (fresh NR, n = 8), mono-cultured NR explants (NR, n = 8), NR explants co-cultured with human bmMSC (NR + MSC, n = 8), and NR explants cultured with medium from NR + MSC co-culture (NR + S, n = 8).

Human bmMSC Immunochemical Evaluation

The bmMSC was fixed with ice-cold methanol (Panreac Quimica SLA, Castellar del Vallès, Spain) at 4°C for 15 minutes. The human bmMSC immunochemical evaluation was performed with a human MSC characterization kit (SCR067; Millipore, Billerica, MA, USA). Primary antibodies (Table) were incubated overnight in a ratio of 1:500 at 4°C. The corresponding species-specific secondary antibody conjugated to Alexa Fluor 488 (green, 1:200; Molecular Probes, Eugene, OR, USA) was incubated for two hours at room temperature. Finally, the nuclei were stained with 10 µg/mL of 4′, 6-diamidino-2-phenylindole (DAPI) (Molecular Probes), and coverslips were mounted onto microscope slides in the presence of fluorescent mounting medium (Dako, Glostrup, Denmark).

Immunochemical Characterization of NR Morphology, Apoptosis, Necroptosis, and Autophagy

NR explants were fixed with 4% paraformaldehyde (Panreac Quimica SLA) in phosphatase-buffered saline solution (PBS) for 24 hours at 4°C. Samples were washed three times in PBS at 4°C. NR explants were cryoprotected in 15% sucrose in PBS for two hours at 4°C, 20% sucrose for two hours at 4°C, and 30% sucrose in PBS for 12 hours at 4°C. Finally, the

Table. Primary Antibodies and Their Experimental Conditions

Molecular Marker	Antibody Origin	Source	Working Dilution	Incubation Time	Incubation Temperature
Human bone marrow mesenchymal stem cells					
Cluster of differentiation present on B-lymphocytes (CD19)	Monoclonal mouse	Millipore, #SCR067	1:500	12 hours	4°C
Cluster of differentiation present on leukocytes (CD14)	Monoclonal mouse	Millipore, #SCR067	1:500	12 hours	4°C
Homing cell adhesion molecule (H-CAM or CD44)	Monoclonal mouse	Millipore, #SCR067	1:500	12 hours	4°C
Melanoma cell adhesion molecule (M-CAM or CD146)	Monoclonal mouse	Millipore, #SCR067	1:500	12 hours	4°C
Thy-1 cell surface antigen (THY-1 or CD90)	Monoclonal mouse	Millipore, #SCR067	1:500	12 hours	4°C
Neuroretinal explants					
GFAP	Polyclonal rabbit	Dako Cytomation Inc, n1506	1:250	1 hour	RT
Vimentin (V9)	Monoclonal mouse	Santa Cruz Biotechnology, SC-6260	1:200	1 hour	RT
PNA lectin	Arachis hypogaea	Molecular Probes Inc, L-21458	1:100	1 hour	RT
PKCα	Polyclonal rabbit	Santa Cruz Biotechnology, #SC-108000	1:100	12 hours	RT
Rho	Polyclonal rabbit	Chemicon-Millipore, AB9279	1:100	12 hours	4°C
RNA binding protein fox-1homolog (RBFOX3/NeuN)	Polyclonal mouse	Merck-Millipore, ABN78	1:150	1 hour	RT
AIF	Polyclonal mouse	Sigma-Aldrich, HPA030611	1:100	24 hours	4°C
Cleaved caspase-3 (Casp3)	Polyclonal rabbit	Cell Signaling Technology, D175	1:100	24 hours	4°C
TUNEL detection kit	—	Roche Diagnostics, 11684795910	1:10	1 hour	RT
MLKL	Polyclonal mouse	Sigma-Aldrich, SAB1408428	1:200	24 hours	4°C
P62	Polyclonal mouse	Abcam, AB56416	1:150	24 hours	4°C

RT, room temperature.

explants were embedded in the Tissue-Tek OCT compound (Sakura Finetek Europe, Alphen, the Netherlands) and cut into 12 µm sections on a cryostat (CM1900; Leica Microsystems, Wetzlar, Germany). Tissue sections were collected onto microscope slides, air-dried, and stored at −20°C until use.

Frozen NR sections were thawed, washed with water, and blocked with 5% goat serum (Sigma-Aldrich) and 0.1% Triton X-100 (Sigma-Aldrich) in PBS for two hours at room temperature (RT). The Table shows the primary antibodies used and their conditions. Briefly, the immunoreactivity of glial fibrillary acidic protein (GFAP), vimentin (Vim), peanut agglutinin (PNA) lectin, protein kinase C α isoform (PKCα), rhodopsin (Rho) protein, neuronal-specific nuclear protein (NeuN), apoptosis-inductor factor (AIF), cleaved caspase-3 (Casp-3), mixed lineage kinase domain-like (MLKL) protein and p62 protein were analyzed. The species-specific secondary antibody conjugated to Alexa Fluor 568 (red, 1:200; Molecular Probes) was incubated for two hours at room temperature. DAPI was used to visualize the nuclei. Finally, the samples were mounted in fluorescent mounting medium and coverslipped. All experiments were conducted in triplicate with four samples/experimental conditions. Control samples in which the primary antibodies were omitted were processed in parallel, and no immunoreactivity was found in any case.

Nuclei Quantification

We performed a manual nuclei cell counting (nuclei/µm^2) for each retinal nuclear layer on magnification × 40 confocal micrographs derived from non-serial DAP-immunostained neuroretinal cryosections (n = 8 cryosections/experimental condition), using the ImageJ software (1.49 version; National Institutes of Health, Bethesda, MD, USA). Afterward, to quantify the number of retinal ganglion cells (RGC), we correlated the number of NeuN-labeled with the number of DAPI-immunostained nuclei in RGL. A single masked researcher performed both analyses.

TdT-mediated dUTP Nick-end Labeling (TUNEL) Immunochemical Analysis

The TUNEL kit for detection of apoptosis labels DNA strand breaks was used. The assay was performed according to the manufacturer's instructions. In brief, frozen NR sections were washed in water and blocked with 5% goat serum (Sigma-Aldrich) 0.1% of Triton X-100 (Sigma-Aldrich) in PBS for two hours at RT. Afterward, TUNEL was incubated under the conditions detailed in the Table. Finally, DAPI immunostaining was used to visualize nuclei. TUNEL analysis was performed in triplicate with four samples/each experimental condition. Control slides in which primary antibodies were omitted were also processed in parallel. To quantify the TUNEL assay, immunofluorescence micrographs were acquired at the same levels of exposure, intensity, and gain (magnification × 40 images; n = 8 sections per experimental condition). Then, the TUNEL-stained nuclei were manually counted in each nuclear layer using the software ImageJ (1.49 version; National Institutes of Health). Finally, the TUNEL-labeled nuclei were correlated with the total DAPI-stained nuclei to obtain quantifiable results expressed as arbitrary units (AU). A single masked researcher performed this analysis.

Immunofluorescence Image Acquisition

Fluorescence images were captured with a Leica TCS SP8 Lightning confocal microscope (Leica Microsystems) and analyzed with Leica LAS AF software. The final processing and composition of the figures were performed with Pixelmator 3.8.2 Phoenix Software (Pixelmator Team, Vilnius, Lithuania).

RNA Extraction, Reverse Transcription, and Real-time Quantitative PCR

Fresh and cultured NR explants were submerged in RNA stabilizing solution (RNAlater, Invitrogen) and stored at −80°C until RNA extraction, which was performed using Trizol reagent (Invitrogen), according to the manufacturer's protocol. RNA quantity and purity were determined by absorbance at 260–280 nm in a spectrophotometer (NanoDrop 2000, Thermo, Waltham, MA, USA).

Complementary DNA (cDNA) was synthesized by reverse transcription using a High Capacity cDNA Reverse Transcription Kit (Applied Biosystems, Foster City, CA, USA) following the manufacturer's manual for the mRNA expression analysis. Relative quantitative real-time polymerase chain reaction (qPCR) was performed using SYBR Green PCR master mix (Applied Biosystems) and porcine-specific primer sets (Supplementary Table S1). The qPCR experiments were conducted using the Applied Biosystems 7500 Real-Time PCR System under the following conditions: 95°C for 10 minutes, 40 cycles of 95°C for 15 seconds, 60°C for one minute, and a final melting curve step. Melting curve analysis was performed to detect the primer specificity. *GAPDH* was used as a housekeeping gene to normalize the expression level of mRNA. The threshold cycle (i.e., the number of cycles to reach the detection threshold) was determined for each reaction, and gene expression was quantified using the $2^{-\Delta\Delta Ct}$ method.[18] All qPCR reactions were performed in triplicate with four samples/experimental conditions.

The relative mRNA expression was analyzed for apoptosis-related genes (B-cell lymphoma 2 [*BCL2*]; *BCL2*-associated X [*BAX]; caspase 3, 8,* and *9 [CASP3, CASP8*, and *CASP9*]), necroptosis-related genes (*MLKL*, receptor-interacting serine/threonine-protein kinase 1 and 3 [*RIPK1* and *RIPK3*]), autophagy-related genes (autophagy-related 7 [*ATG7*], coiled-coil moesin-like *BCL2* interacting protein [*BECLIN1*]; sequestosome1 [*SQSTM1*]; mammalian target of rapamycin [*mTOR*]; autophagy marker light chain 3B [*LC3B*]), inflammation-related genes (interleukin 1, 6, and 10 [IL1, IL6, and IL10]; transforming growth factor beta 1 [TGFb1] and tumor necrosis factor α [TNFα]), and oxidative stress-related genes (cyclooxygenase 2 [COX2]; cytochrome B-245 beta chain [CYBB]; glutathione peroxidase 6 [GPX6]; superoxide dismutase 1 [SOD1]; thioredoxin 2 [TXN2]; and thioredoxin reductase 1 [TXNRD1]).

Statistical Analysis

Continuous variables are expressed as the mean ± standard deviation. The Kolmogorov-Smirnov test was used to analyze the distribution of continuous variables. In the case of parametric variables, the analysis of variance (ANOVA) *t*-test was applied. In the case of nonparametric variables, groups were compared using the Mann-Whitney U-test (two groups) or the Kruskal–Wallis test (more than two groups). $P < 0.05$ was considered significant. All analyses were performed using the SPSS version 22.0 statistical package (SPSS, Chicago, IL, USA).

Results

Human bmMSC Surface Marker Evaluation

The human bmMSC culture reached confluence before coculturing with the NR explants, and the bmMSC viability exceeded 95%. The immunochemical bmMSC surface marker evaluation showed that mono- and co-cultured bmMSCs were positive for CD44, CD90, and CD146 and negative for CD14 and CD19 surface proteins (Fig. 1).

NR Morphology Immunochemical Evaluation

Because PNA lectin binds to the extracellular matrix of the cone outer segment,[19] it was used to identify and evaluate the cones (Figs. 2A–D). In the fresh NR explants, the immunoreactivity of PNA lectin was restricted to and uniformly distributed in the cone outer segment (Fig. 2A). The PNA lectin immunoreactivity in NR explants cultured alone was scarcely detectable due to marked cone degeneration (Fig. 2B). PNA lectin immunoreactivity in NR + MSC and NR + S was similar to fresh NR explants (Figs. 2C,

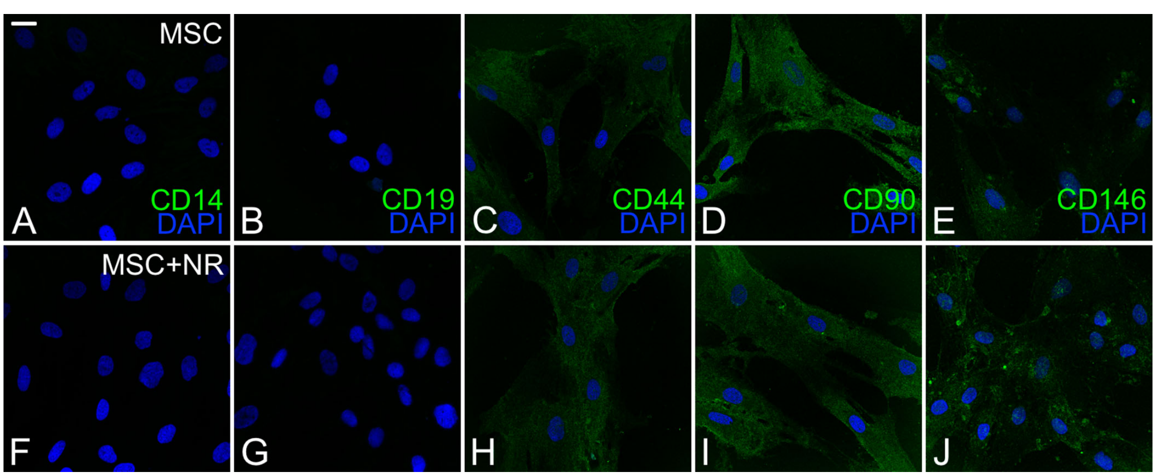

Figure 1. Human bmMSC surface marker evaluation. MSC surface markers after 72 hours of culture (**A,** CD14; **B,** CD19; **C,** CD44; **D,** CD90; and **E,** CD146) and after 72 hours of co-culture with NR explants (**F,** CD14; **G,** CD19; **H,** CD44; **I,** CD90; and **J,** CD146). *Scale bar*: 25 μm.

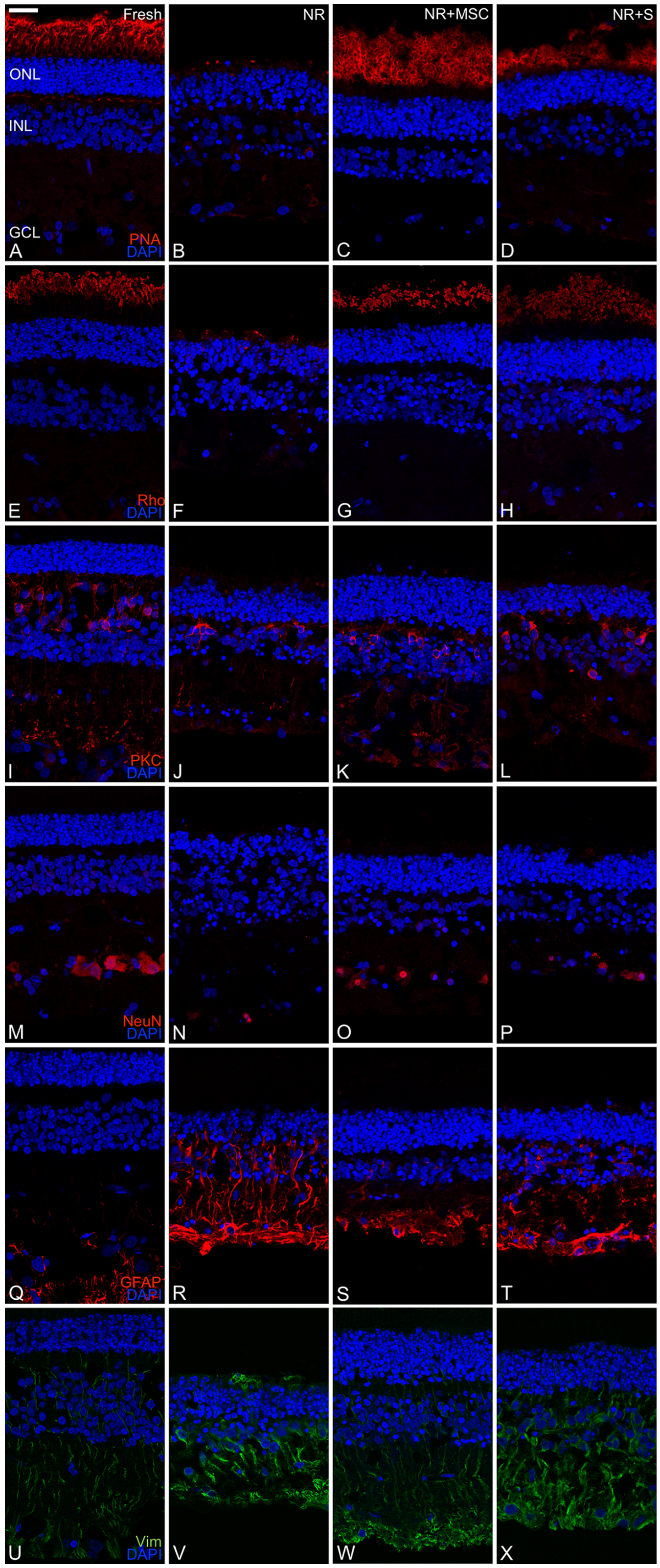

Figure 2. NR morphology immunochemical evaluation. Immunoreactivity of PNA lectin (**A–D**), rho protein (**E–H**), PKC α isoform (PKCα) (**I–L**), NeuN (**M–P**), GFAP (**Q–T**) and Vim (**U–X**). The experimental conditions analyzed were fresh neuroretinas (Fresh), mono-cultured NR explants for 72 hours (NR), NR explants co-cultured with human bmMSC for 72 hours (NR + MSC), and NR explants cultured with medium from NR + MSC co-culture for 72 hours (NR + S). *Scale bar*: 25 µm.

2D). However, the PNA distribution pattern, which differed from the fresh NR explants, indicates incipient degenerative processes in the cones.

To identify and study the rods, the immunoreactivity of Rho protein was analyzed (Figs. 2E–H). Rho protein is transported to the connecting cilium and inserted into newly formed membrane discs at the base of the outer segment; thus, Rho protein is homogenously located in the rod external discs,[20] as observed in the fresh NR samples (Fig. 2E). In NR mono-cultured explants, Rho protein immunoreactivity was hardly detectable in this experimental setup and restricted to the remaining degenerated rods (Fig. 2F). The Rho immunoreactivity in the NR + MSC and NR + S remains the fresh NR explants (Figs. 2G, 2H); although, as shown in the cone study, Rho distribution resembles the initial signs of rod degeneration (Fig. 2H).

The immunoreactivity of PKCα was determined to analyze the morphology of the rod bipolar cells (Figs. 2I–L). PKCα is crucial for regulating rod bipolar cell function and accelerates the glutamate-driven signal transduction and termination.[21] In the fresh NR explants, the immunoreactivity of PKCα was distributed uniformly along with the bipolar cells through the inner nuclear layer (INL) and the inner and outer plexiform layers (IPL and OPL) (Fig. 2I). The immunoreactivity distribution of PKCα in NR monoculture explants was heterogeneous (Fig. 2J). The distribution of PKCα in NR + MSC and NR + S remains the fresh NR explants but with a more dispersed distribution at the terminal buttons (Figs. 2K, 2L).

NeuN is an RNA-binding protein that allow studying ganglion cells[22] as observed in the fresh NR explants (Fig. 2M). NeuN protein immunoreactivity was detected partially at the ganglion cell layer (GCL) in the NR + MSC and NR + S but was nearly absent in the NR explants mono-cultured for 72 hours (Figs. 2M–P). To perform a more accurate analysis of RGC, we quantified NeuN labeled cells. NeuN quantification showed that the number of RGC was significantly decreased in NR monocultured compared to all the other experimental conditions. There were no statistical differences between NR + MSC and NR + S or fresh NR (Supplementary Fig. S1).

Finally, we quantified the DAPI-positive nuclei in every retinal nuclear layer (Supplementary Fig. S2). In the total retina, all experimental conditions presented a higher number of nuclei than NR monocultured, NR + MSC was higher than NR + S, and no significant difference was found with fresh NR (Supplementary Fig. S2A). In the ONL, fresh NR and NR + MSC were significantly higher than NR monocultured, NR + MSC was higher than NR + S, and there were no statistical differences between fresh NR and NR + MSC nor NR monocultured and NR + S (Supplementary Fig. S2B). In the INL, all experimental conditions were higher than NR monocultured; fresh NR was higher than NR + S, and no statistical differences were found between fresh NR and NR + MSC nor NR + MSC and NR + S (Supplementary Fig. S2C). In the GCL, the only significant differences were that fresh NR was higher than NR monocultured and NR + S (Supplementary Fig. S2D).

Characterization of the Gliosis: GFAP and Vimentin Immunoreactivity

The immunoreactivity of GFAP was analyzed for assessing retinal gliosis, a sign of retinal degeneration (Figs. 2Q–T).[5] Gliosis results from glial cell activation, in which GFAP is upregulated in Müller cells.[23,24] The GFAP immunoreactivity in the fresh NR explants was mainly restricted to the nerve fiber layer (NFL) and GCL (Fig. 2Q). In the NR explants cultured alone, GFAP immunoreactivity is present in INL and the outer nuclear layer (ONL) (Fig. 2R). In the case of NR + MSC, GFAP immunoreactivity was distributed throughout the GCL, IPL, and the innermost INL region (Fig. 2S). Finally, the immunoreactivity of the GFAP in the NR + S extended from the NFL to the INL (Fig. 2T).

We also performed an immunohistochemical analysis of the specific Müller cell marker, Vimentin (Vim)[25] (Figs. 2U–X). In fresh NR, NR + MSC, and NR + S, the immunoreactivity of Vim was distributed through the inner limiting membrane (ILM) and the outer limiting membrane (Figs. 2U–W). In NR monocultured, the Vim immunoreactivity is upregulated and seems to reach the photoreceptors IS (Fig. 2X).

Apoptosis, Necroptosis, and Autophagy

The AIF protein, which is involved in intrinsic apoptotic signals, is a mitochondrial protein primarily in the photoreceptor cells and the cytoplasm of other retinal cells during retinal degeneration.[26] Immunohistochemical evaluation of AIF protein showed that the immunoreactivity in the fresh NR explants was restricted to the GCL (Fig. 3A); meanwhile, AIF immunoreactivity in NR mono-cultured, NR + MSC, and NR + S was preponderant the photoreceptors IS (Figs. 3B–D). Casp-3 is the primary protein that executes apoptosis.[5] In fresh NR, the immunoreactivity of Casp-3 was not detectable (Fig. 3E); in NR monocultured, the Casp-3 immunoreactivity was upregulated and disseminated through all the NR tissue (Fig. 3F). In the case of NR + MSC, it was detected between GCL and INL (Fig. 3G); meanwhile, in NR + S, it was detected between GCL and OPL (Fig. 3H).

TUNEL detection kit labels DNA strand breaks in cells that undergo apoptosis.[27] TUNEL immunoreactivity was not detectable in fresh NR (Fig. 3I). In the case of NR monocultured, TUNEL immunoreactivity was detectable between the GCL and the OPL (Fig. 3J); meanwhile in NR + MSC mainly was focused on the ONL (Fig. 3K) and NR + SB between INL and photoreceptor IS (Fig. 3L). Furthermore, to quantify the apoptosis rate in each retinal layer per experimental condition, we performed the TUNEL assay quantification. The apoptosis rate in the total retina, GCL, and INL was significantly higher in NR monocultured, and there was no difference between fresh NR, NR + MSC, and NR + S (Supplementary Figs. S3A, C–D). In the ONL, there were no statistical differences between NR monocultured, NR + MSC, and NR + S, and all of them were significantly higher than fresh NR (Supplementary Fig. S3B).

The MLKL-RIPK pathway is associated with necroptotic pathway activation.[28] Immunoreactivity distribution of the MLKL protein in the fresh NR explants was mainly restricted to GCL (Fig. 3E). The MLKL immunoreactivity was distributed all over the tissue of NR mono-cultured, NR + MSC, and NR + S, being predominant in photoreceptors IS (Figs. 3F–H).

The p62 protein expression can be used to monitor autophagy because it is degraded during autophagy.[29] The immunochemical analysis of p62 protein showed that the immunoreactivity was barely detectable and distributed all over the retinal tissue in all experimental conditions (Figs. 3I–L). The relative mRNA expressions of genes involved in

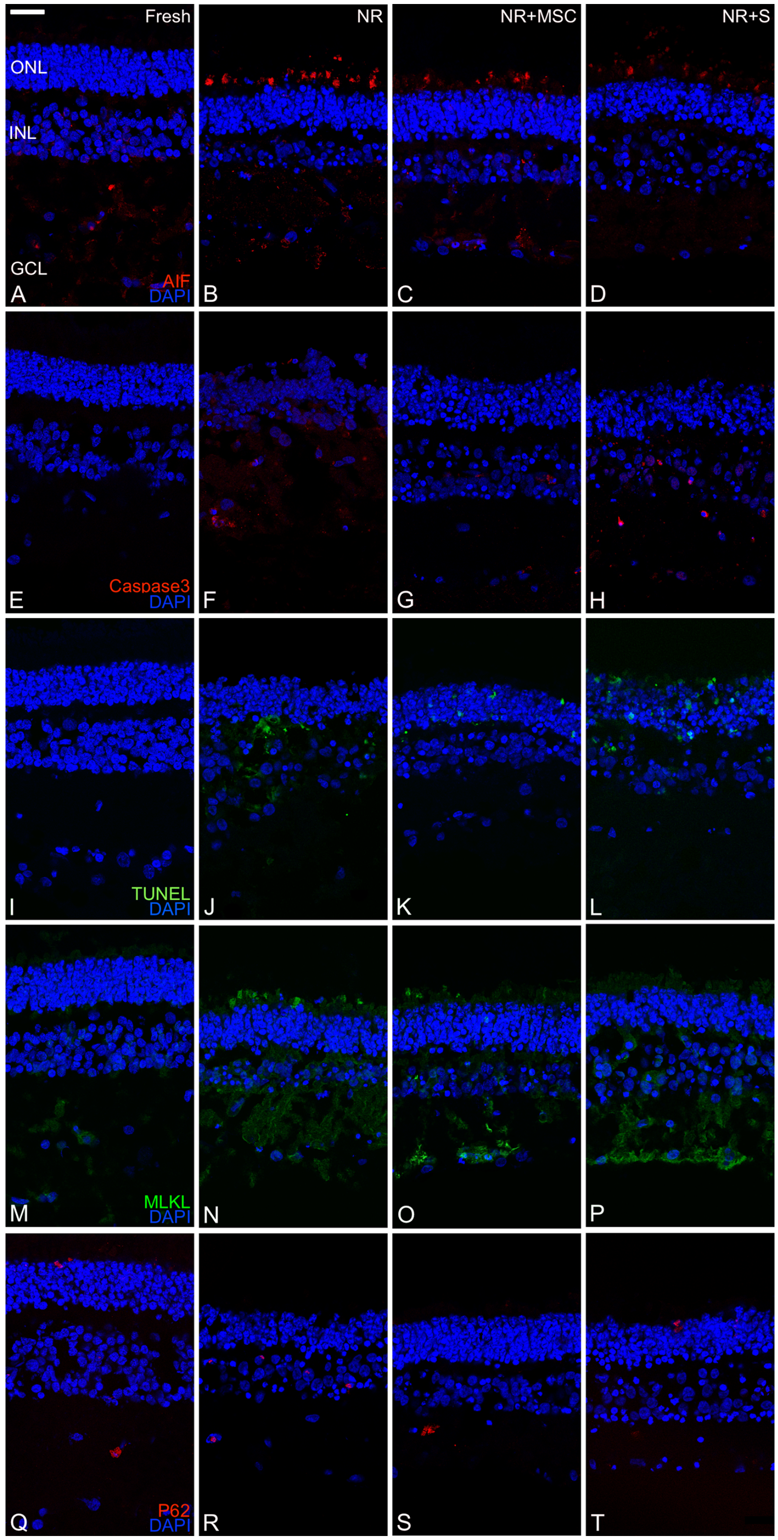

Figure 3. Immunochemical apoptosis, necroptosis, and autophagy characterization. Immunoreactivity of AIF (**A–D**), Casp-3 protein (**E–H**), TUNEL assay (I-L), MLKL (M-P), p62 (Q-T). The experimental conditions analyzed were fresh neuroretinas (Fresh), mono-cultured NR explants for 72 hours (NR), NR explants co-cultured with human bmMSC for 72 hours (NR + MSC), and NR explants cultured with medium from NR + MSC co-culture for 72 hours (NR + S). *Scale bar*: 25 µm.

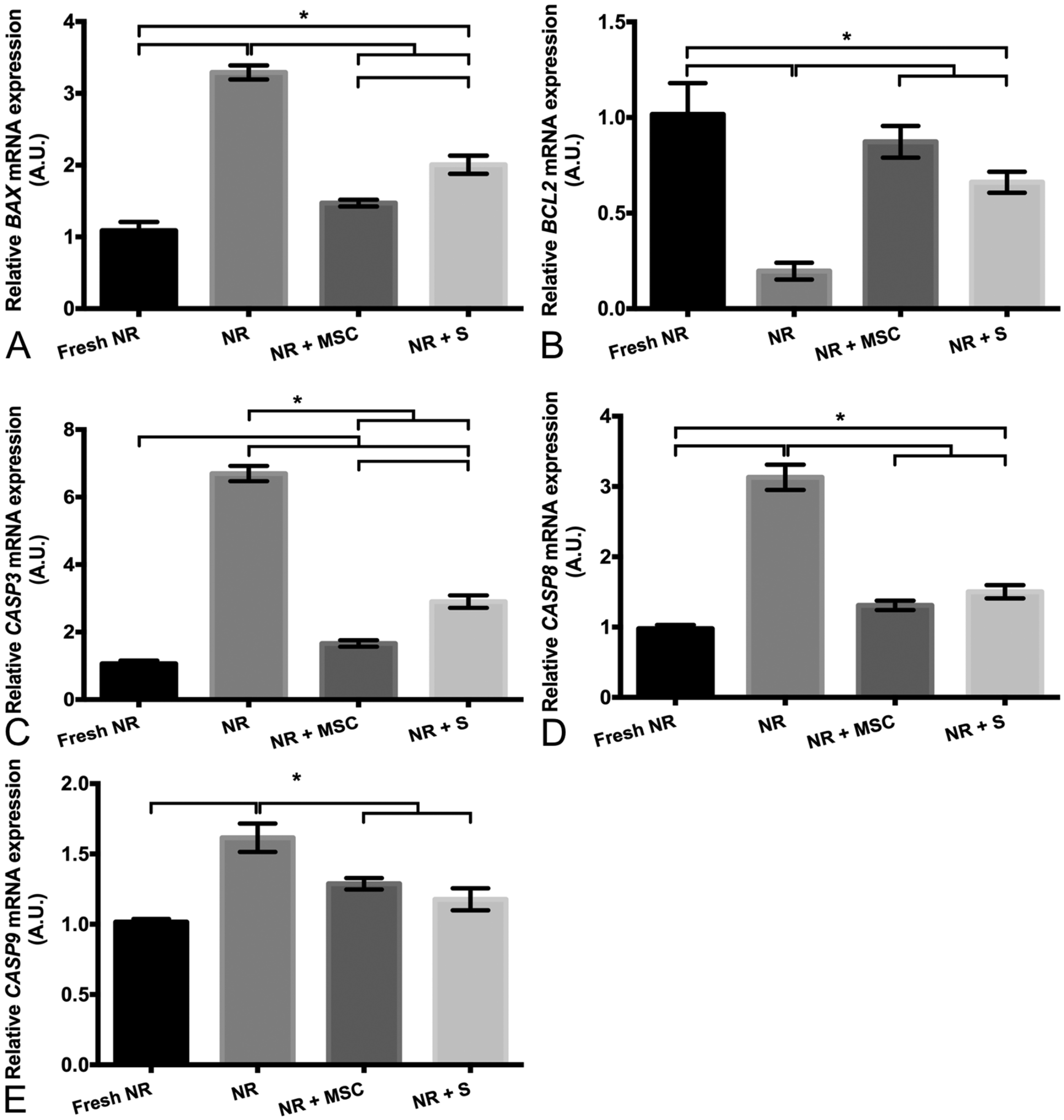

Figure 4. Relative mRNA expressions of apoptosis-related genes in NR explants. Relative mRNA expressions of the *BAX* gene (**A**), *BCL2* gene (**B**), *CASP3* gene (**C**), *CASP8* gene (**D**), and *CASP9* gene (**E**). The experimental conditions analyzed were fresh NR explants (Fresh), mono-cultured NR explants for 72 hours (NR), NR explants co-cultured with human bmMSC for 72 hours (NR + MSC), and NR explants cultured with medium from NR + MSC co-culture for 72 hours (NR + S). $^*P < 0.05$, AU: arbitrary units. Bars represent mean values and their respective standard deviation. Kolmogorov-Smirnov test and ANOVA *t*-test were applied.

apoptosis, necroptosis, and autophagy were evaluated to confirm the results.

The relative mRNA expressions of the *BAX*, *BCL2*, *CASP3*, *CASP8* and *CASP9* genes were studied in the NR explants to analyze apoptosis (Fig. 4). The relative mRNA expressions of *BAX*, *CASP3*, *CASP8,* and *CASP9* in the NR explants cultured for 72 hours are significantly increased compared to fresh NR, NR + MSC, and NR + S explants. The relative mRNA expression of *BCL2* decreased significantly in NR explants cultured for 72 hours compared to the fresh NR, NR + MSC, and NR + S explants. The relative mRNA expressions of *BAX*, *BCL2*, *CASP8* and *CASP9* genes were similar in the fresh NR and NR + MSC explants. In the *CASP3* gene, the relative mRNA expression was higher in the NR + MSC than in fresh NR explants; a comparison of these two showed that the relative mRNA expression was only comparable to the *CASP9* gene. Finally, the relative mRNA expressions of *BCL2*, *CASP8,* and *CASP9* were similar in the NR + MSC and NR + S experimental conditions.

The relative mRNA expressions of the *RIPK1*, *RIPK3,* and *MLKL* genes were analyzed to study necroptosis, and the results (Fig. 5) showed that the necroptosis-related gene relative mRNA expression was significantly higher in the NR explants cultured for 72 hours compared with the fresh NR, NR + MSC, and NR + S explants. The relative mRNA expressions of the *MLKL* and *RIPK3* genes were similar in the fresh NR and NR + MSC explants; the *RIPK1* gene expression was significantly higher in the NR + MSC explants. A comparison of the fresh NR and NR + S explants showed that the relative mRNA of all necroptosis-related genes was significantly

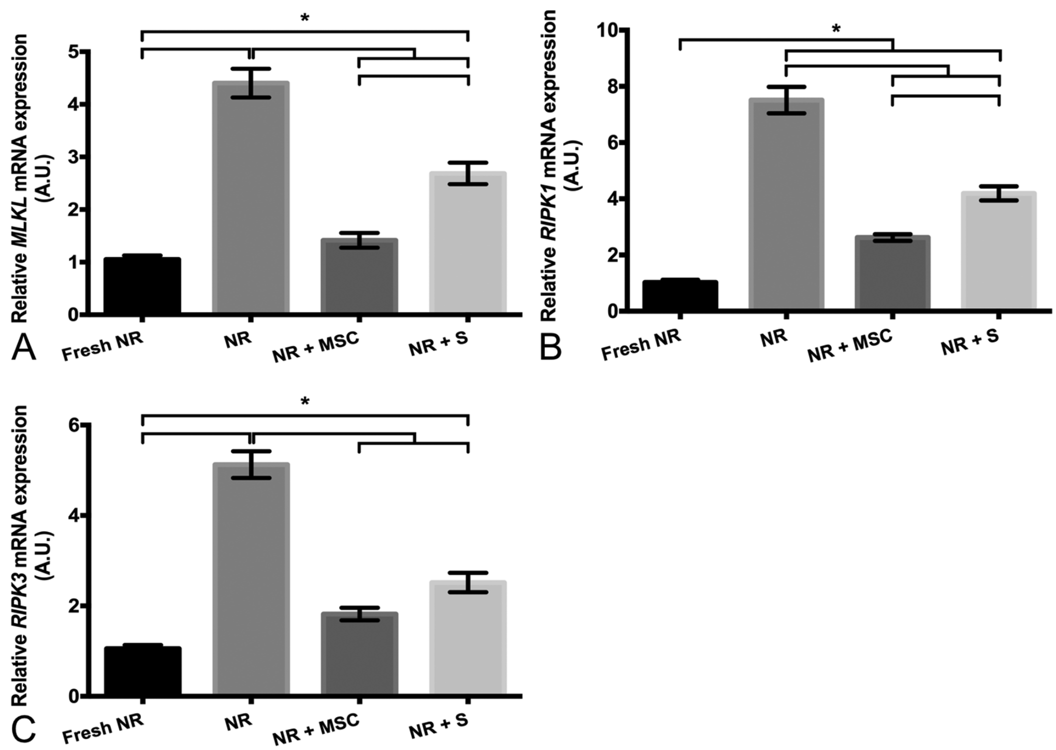

Figure 5. Relative mRNA expressions of necroptosis-related genes in NR explants. Relative mRNA expressions of the *MLKL* gene (**A**), *RIPK1* gene (**B**), and *RIPK3* gene (**C**). The experimental conditions analyzed were fresh NR explants (Fresh), mono-cultured NR explants for 72 hours (NR), NR explants co-cultured with human bmMSC for 72 hours (NR + MSC), and NR explants cultured with medium from NR + MSC co-culture for 72 hours (NR + S). $^*P < 0.05$, AU: arbitrary units. *Bars* represent mean values and their respective standard deviation. Kolmogorov-Smirnov test and ANOVA *t*-test were applied.

higher in the latter. In the NR + MSC and NR + S experimental conditions, the relative mRNA expression was close only to the *RIPK3* gene.

The relative mRNA expressions of the *ATG7*, *BECLIN1, LC3B*, *mTOR,* and *SQSTM1* genes were analyzed in the NR explants to study autophagy (Fig. 6). The results showed that the relative mRNA expressions of the *ATG7* and *BCLIN1* genes were significantly increased in all experimental conditions compared to the fresh NR explants. The expressions of the *LC3B*, *mTOR,* and *SQSTM1* genes decreased significantly in all experimental conditions compared to the fresh NR explants. The *ATG7* and *BCLIN1* relative mRNA expressions were significantly lower in the NR + MSC than in the NR explants cultured for 72 hours. In the *LC3B* and *SQSTM1* genes, the mRNA expression was significantly higher in the NR + MSC than in the NR explants cultured alone. The relative expressions of the *LC3B* and *SQSTM1* genes also were significantly higher in the NR + S experimental condition than in the NR explants cultured for 72 hours. The *ATG7*, *BECLIN1,* and *mTOR* relative mRNA gene expressions were similar between the NR + S and NR explants cultured alone. The expression of all autophagy-related genes analyzed was similar in the NR + MSC and NR + S experimental conditions.

Analysis of the Relative mRNA Expression of the Oxidative Stress and Inflammation-Related Genes

The relative mRNA expressions of the *TXN2, GPX6, SOD1, COX2*, *CYBB*, *CYBA,* and *TXNRD1* genes involved in the oxidative stress process (Fig. 7) showed that the mRNA expressions of the *COX2*, *CYBA,* and *TXNRD1* genes increased significantly in all experimental conditions compared to the fresh NR explants. The expression of the *SOD1* gene increased significantly in the NR + MSC and NR + S explants compared with the fresh NR explants. It decreased significantly in the NR explants cultured alone compared with the fresh NR explants. In the fresh NR and NR explants cultured alone, the relative mRNA expression was comparable in the *GPX6* and *TXN2* genes. The *CYBB* gene expression increased significantly in the NR explants cultured alone for 72 hours. The *CYBB* relative mRNA expression was similar in the fresh NR and NR + MSC experimental conditions; the *GPX6* and *TXN2* expression gene expressions increased significantly in the NR + MSC explants. A comparison of fresh NR and NR + S explants showed that the *TXN2* mRNA expression was similar, and the expressions of the *CYBB* and *GPX6* genes increased significantly in the NR + S condition. The relative mRNA expressions of the *COX2*, *CYBA,* and *TXNRD1* genes were similar in the NR + MSC, and NR + S explants versus the NR explants cultured alone; the *GPX6* and *SOD1* expressions were significantly higher in the NR + MSC and NR + S experimental conditions than in the NR mono-cultured explants. The expression of the *CYBB* gene was similar in the NR + S and NR explants cultured alone.

Finally, the relative expressions of the *IL1*, *IL6*, *IL10*, *TGF*b*1,* and *TNFα* genes were analyzed to study the inflammatory process (Fig. 8). The relative expressions of the inflammation-related genes increased significantly in all experimental conditions compared to the fresh NR explants.

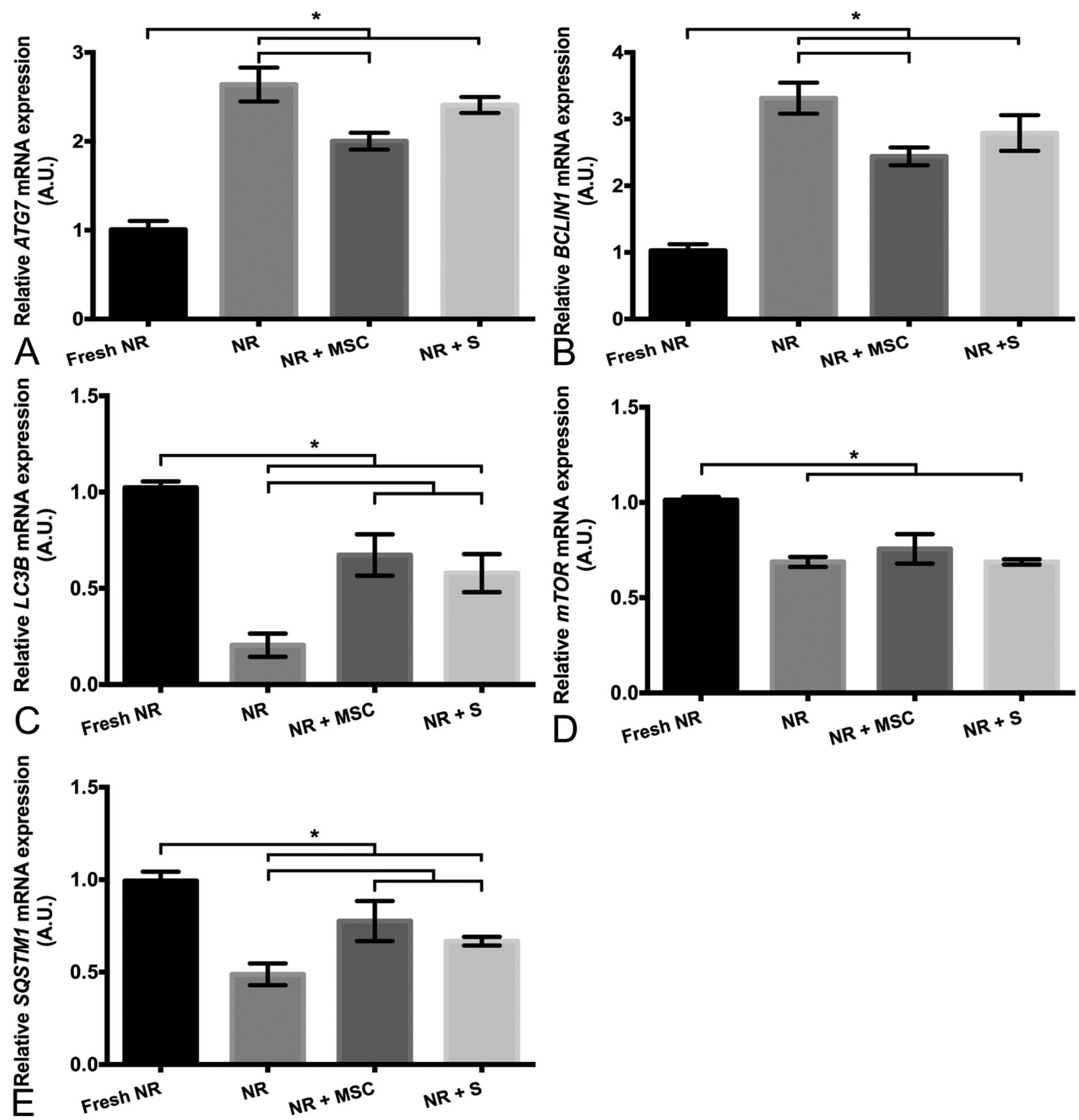

Figure 6. Relative mRNA expressions of autophagy-related genes in NR explants. Relative mRNA expressions of the *ATG7* gene (**A**), *BECLIN1* gene (**B**), *LC3B* gene (**C**), *mTOR* gene (**D**), and *SQSTM1* gene (**E**). The experimental conditions analyzed were fresh NR explants (Fresh), mono-cultured NR explants for 72 hours (NR), NR explants co-cultured with human bmMSC for 72 hours (NR + MSC), and NR explants cultured with medium from NR + MSC co-culture for 72 hours (NR + S). *$P < 0.05$, AU: arbitrary units. *Bars* represent mean values and their respective standard deviation. Kolmogorov-Smirnov test and ANOVA *t*-test were applied.

No other comparisons identified significant differences in the relative mRNA expression of the inflammation-related genes.

Discussion

No cures are available for most RND, and cell-based therapy using human bmMSC, as a source of secretion of neuroprotective, anti-inflammatory, anti-apoptotic, and immunomodulating factors, among others, may be promising therapeutic options.[7,8] We showed previously that intravitreal injection of human bmMSC is safe and well tolerated and that the cells are present in the vitreous cavity for 2 to 4 weeks.[15] Therefore, the primary approach of MSC cell therapy is neuroprotective through their paracrine properties; and the development of therapeutic strategies based on the neuroprotective capacity of MSC secretome is being studied extensively.[13,14] Therefore the current study evaluated the neuroprotective capacity of human bmMSC secretome obtained under conditions of NR degeneration and sought to determine if this specific secretome modulates the retinal response to neurodegeneration. To the best of our knowledge, this study is the first to analyze the ability of human bmMSC secretome (obtained in NR degeneration environment) to modulate the retinal response to neurodegeneration, which is crucial in the development of therapeutic strategies based on the production of "MSC secretome cocktails" with neuroprotective properties. The production of secretome cocktails may facilitate the development of cell-free compositions with neuroprotective capabilities and have significant advantages over using living cells in clinical practice.[13]

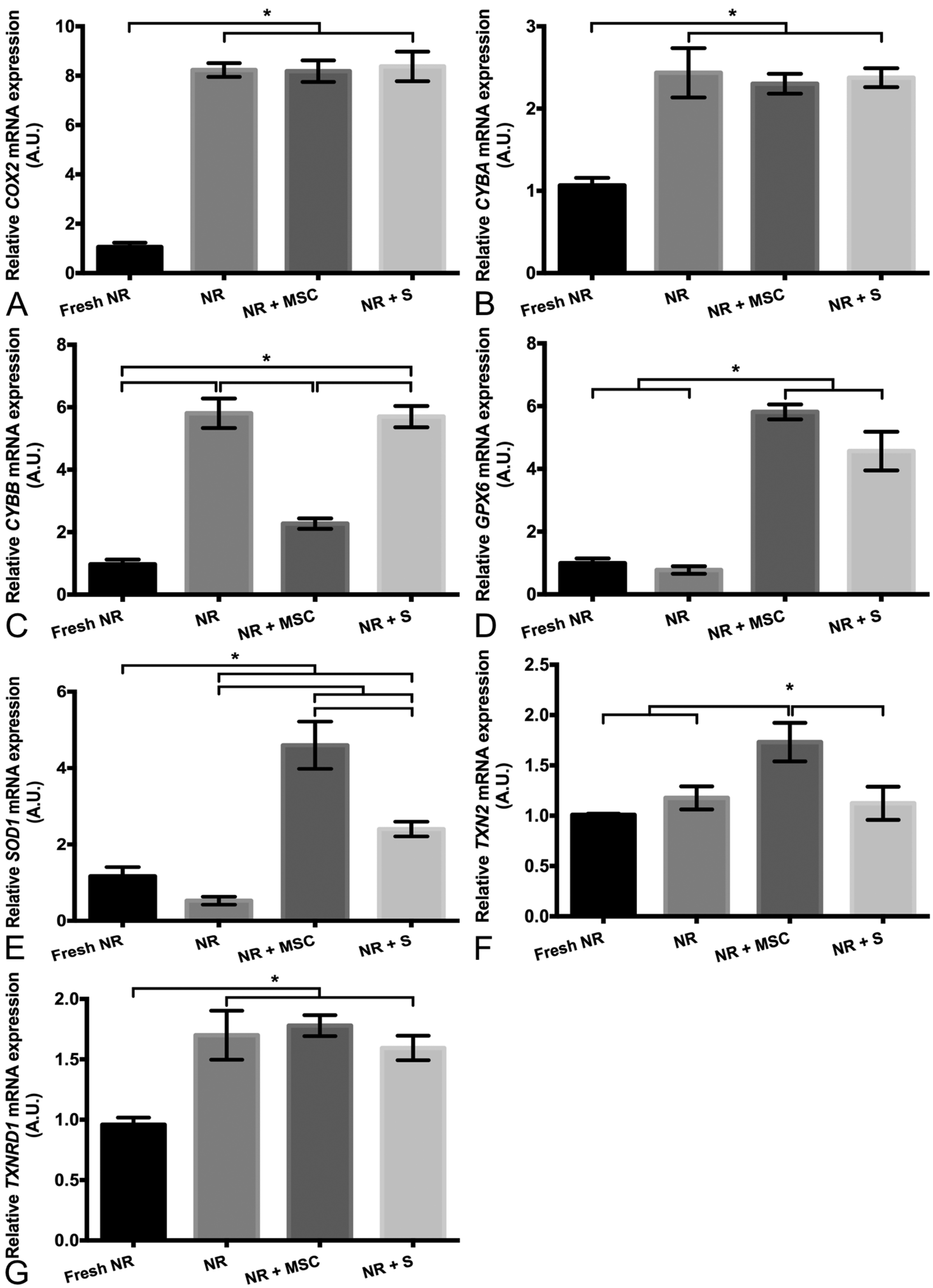

Figure 7. Relative mRNA expressions of oxidative stress-related genes in NR explants. Relative mRNA expressions of the *COX2* gene (**A**), *CYBA* gene (**B**), *CYBB* gene (**C**), *GPX6* gene (**D**), *SOD1* gene (**E**), *TXN2* gene (**F**), and *TXNRD1* gene (**G**). The experimental conditions analyzed were fresh NR explants (Fresh), mono-cultured NR explants for 72 hours (NR), NR explants co-cultured with human bmMSC for 72 hours (NR + MSC), and NR explants cultured with medium from NR + MSC co-culture for 72 hours (NR + S). *$P < 0.05$, AU: arbitrary units. *Bars* represent mean values and their respective standard deviation. Kolmogorov-Smirnov test and ANOVA *t*-test were applied.

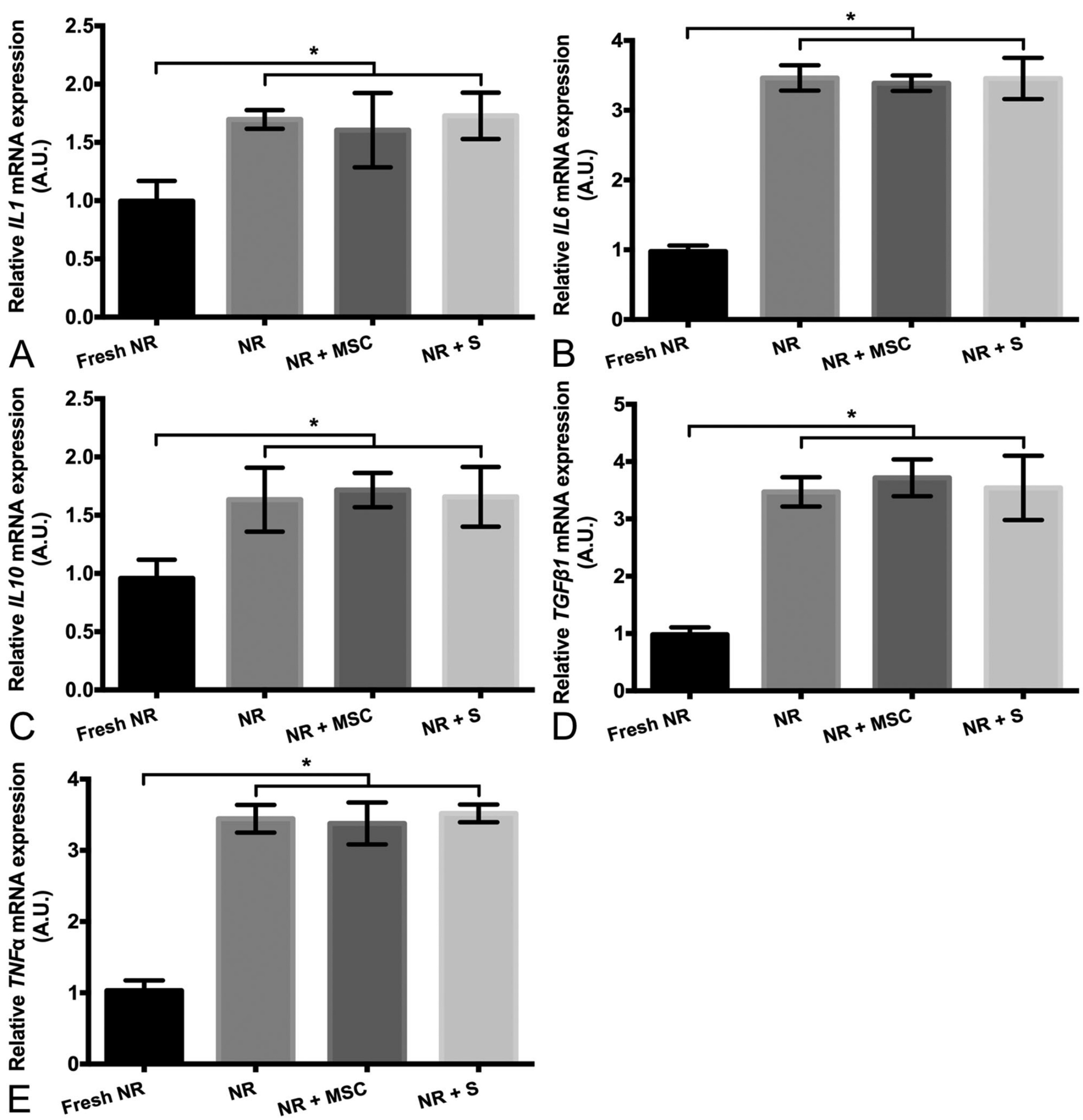

Figure 8. Relative mRNA expressions of inflammation-related genes in NR explants. Relative mRNA expressions of the *IL1* gene (**A**), *IL6* gene (**B**), *IL10* gene (**C**), *TGFb1* gene (**D**), and *TNFa* gene (**E**). The experimental conditions analyzed were fresh NR explants (Fresh), mono-cultured NR explants for 72 hours (NR), NR explants co-cultured with human bmMSC for 72 hours (NR + MSC), and NR explants cultured with medium from NR + MSC co-culture for 72 hours (NR + S). *$P < 0.05$, AU: arbitrary units. *Bars* represent mean values and their respective standard deviation. Kolmogorov-Smirnov test and ANOVA *t*-test were applied.

The current study used organ retinal explant cultures, which seem to be an excellent tool for studying retinal neurodegeneration and neuroprotection because organ retinal explant cultures replicate the cellular and molecular changes in the in vivo retina neurodegeneration.[17,30] However, in vitro limitations include the absence of blood supply, the axotomy of RGC as part of the dissection procedure, and the absence of retinal pigmented epithelium.[17]

The distributions of PNA lectin, Rho, PKCα, and NeuN protein immunoreactivity were comparable between the neuroretinas cultured with bmMSC and bmMSC secretome. Although both conditions showed incipient NR degeneration, compared with fresh neuroretinas, the neuroprotective effect of human bmMSC secretome over cones, rods, rod bipolar cells, and ganglion cells was highlighted compared with the retinas cultured alone. Besides, the cell loss quantification showed that a reduced number of nuclei was correlated to higher alterations in the immunoreactivity patterns and retinal degeneration. bmMSC and bmMSC secretome displayed the same preservative effect over retinal cells in most retinal nuclear layers, indistinguishable from a fresh NR. Furthermore, the quantification of the NeuN-labeled cell confirmed that the neuroprotective effect of bmMSC and bmMSC secretome are equal for RGC.

The differences between GFAP and Vim immunoreactivity distribution in fresh NR; and the highly correlated immunoreactivity patterns of GFAP and Vim in degenerated NR add evidence to the premise that GFAP is upregulated in gliotic Müller cells during retinal degeneration.[5] Reactive gliosis, and thus NR degeneration,[23,31] is less disseminated in neuroretinas cultured with bmMSC or with only bmMSC secretome compared with neuroretinas cultured alone. The current findings suggested that human bmMSC secretome exhibited a neuroprotective effect over in vitro retinal neurodegeneration, which agreed with previous reports.[11,12,32,33] In this sense, it has been reported that retinal neuroprotection may be a consequence of the paracrine properties of the MSC.[5,10–12]

Oxidative stress is defined as dysregulation between the generation and elimination of reactive oxygen species (ROS). It is widely accepted that ROS damage plays a crucial role in retinal neurodegeneration by promoting inflammation and apoptosis.[34–36] Most cells die by apoptosis during retinal neurodegeneration without damaging the surrounding tissue.[5,37] Necrosis and necroptosis (programmed necrosis) also are involved in apoptosis during retinal neurodegeneration.[38] Our results showed that the human bmMSC secretome modifies the expressions of genes involved in oxidative stress, apoptosis, and necroptosis during in vitro retinal neurodegeneration and may explain the neuroprotective capacity of the bmMSC secretome. Retinal tissue's cellular and molecular responses to neurodegeneration are attempts to preserve the structure and function.[5] The current results suggested that the human bmMSC secretome stimulates that response. The most essential cell antioxidant system is the thioredoxin (Trx) pathway, which regulates the cell redox status.[39,40] TrxR1 is the endogenous regulator of the Trx pathway because it reduces Trx protein and other compounds from detoxifying cells resulting from ROS damage.[41] Trx and TrxR1 are crucial in neuroprotection through the modulation of oxidative stress, inflammation, and anti-apoptotic processes.[42]

Trx2 is another redox protein of the Trx pathway that is crucial for controlling oxidative stress, apoptosis, and cell viability.[43] The association between human *TXN2* gene deficiency and early-onset neurodegeneration has been reported.[44] The current results showed that during in vitro retinal neuroprotection by bmMSC secretome, the expression of the *TXN2* gene increases, which supports the possible essential role of the MSC secretome in activating the antioxidant machinery. *TXNRD1* gene expression also increased in the presence of the bmMSC secretome, but it was similar to that of the mono-cultured retinal explants. Glutathione peroxidases (GPxs) also protect against ROS damage and have a crucial antioxidant capacity in pathological situations.[44] The current results showed increased *GPX6* gene expression in the presence of human bmMSCs, which agreed with the results described previously. An increase in the relative mRNA expression of the *SOD1* gene, which encodes to the superoxide dismutase enzyme involved in destroying free superoxide radicals,[45] also was observed. The current results support the hypothesis that the mechanism of the retinal neuroprotection provided by the human bmMSC secretome may be through activation of the antioxidant machinery to modulate ROS damage. Besides, the bmMSC secretome has an antioxidant effect over neuroretinal degeneration in vitro; however, the effect seems to be better in the presence of cells, probably because MSC constantly secret neurotrophic factors.

Oxidative stress and ROS damage induce apoptosis.[46] As mentioned, apoptosis may be caspase dependent or independent.[47] Caspase-dependent apoptosis pathways are the primary mechanism involved in retinal cell neurodegeneration.[5] Caspase-dependent apoptosis is characterized by all pathways converging on activation of cysteine-aspartic acid proteases (called caspases) that are classified in the initiator caspases (2, 8, 9, and 10) and executor caspases (3, 6, and 7).[48] Apoptosis is exquisitely controlled by the presence of pro-apoptotic proteins (Bax and AIF, among others) and anti-apoptotic factors (e.g., Bcl2) in response to extrinsic or intrinsic stimuli.[47] The current results showed that the expression of pro-apoptotic genes decreased during retinal neuroprotection by bmMSC secretome (*BAX, CASP3, CASP8,* and *CASP9* genes), and the expression of *BCL2*, an anti-apoptotic gene, increased. Besides, the neurotrophic factors of bmMSC and bmMSC secretome seem to limit the immunoreactivity scattering of the apoptotic proteins AIF and Casp-3 to individual retinal layers, suggesting it has anti-apoptotic properties. Moreover, quantification of the apoptosis rate confirmed the anti-apoptotic effect that confers the bmMSC and bmMSC secretome in most of retinal nuclear layers.

Several models of retinal diseases have demonstrated the role of necroptosis, a type of regulated necrosis.[38,49] We observed that the expressions of genes that are crucial to necroptosis activation (*RIPK1*, *RIPK3,* and *MLKL*) decreased in retina explants cultured with bmMSC secretome. Human bmMSC secretome may promote decreased cellular necroptosis activation during retinal neurodegeneration. Analyses of apoptosis and necroptosis cell death pathways showed that the bmMSC secretome prevents retinal cell death by inhibiting programmed apoptotic pathways, thus reinforcing the hypothesis that human MSC secretome exhibits a neuroprotective capacity over retinal degeneration. These results also reinforce the idea that targeting death receptor-induced apoptosis and necroptosis may be a therapeutic strategy to prevent neuronal damage in retinal neurodegeneration.[50] Inhibiting apoptosis or necroptosis is insufficient to avoid neurodegenerative processes because the cellular programmed death pathways compensate for each other.[51] We hypothesize that the bmMSC secretome may modulate all mechanisms involved in neurodegeneration jointly and uniformly and thus exhibit a neuroprotective capability.

Autophagy, which has been reported to be important during retinal degeneration,[37,52] is a lysosomal catabolic process involved in the degradation of damaged organelles and proteins that protect cells against molecular alterations caused by pathologies such as infections, neurodegeneration, and aging.[53,54] Autophagy starts with autophagosome formation, a double membrane structure encapsulating the target. The autophagosome then fuses with lysosomes to degrade its contents. A key regulator of autophagy is mTOR kinase, a principal autophagy inhibitory signal in the presence of growth factors and abundant nutrients. Other critical regulatory molecules that control autophagy include the ULK1 complex, bclin1 protein, and ATG proteins.[55,56] Autophagy is a highly selective catabolic process due to the involvement of LC3 and p62 proteins; a p62-LC3 interaction allows anchoring of p62 to the autophagosome, which enables the degradation of selected proteins.[57] The current results showed that the bmMSC secretome might modify autophagy during retinal neurodegeneration. These results agreed with previous studies that reported the crucial role of autophagy modulation in neuroprotection,[58,59] suggesting that the retinal neuroprotective properties of the human bmMSCs also may be associated with autophagy modulation.

Our previous studies have summarized that bmMSC secrete proteins that may be crucial in retinal neuroprotection in an environment of retinal neurodegeneration. Proteins with anti-inflammatory and anti-apoptotic capacity are directly involved in neuroprotective processes.[11,12] In addition, this study also suggested that the presence of bmMSC is unnecessary and that only the bmMSC secretome may have a neuroprotective effect over retinal neurodegeneration through modulation of oxidative stress, autophagy and programmed apoptosis. These findings support the hypothesis that developing a cell-free therapeutic strategy based on the production of MSC secretome cocktails with neuroprotective characteristics may be an approach to treat RND.[11–14] The results reported here and in our previous studies[11,12,60] showed that the neuroprotective capacity of bmMSC secretome is higher than that of the secretome from adipose MSCs. In addition, an environment of retinal neurodegeneration, as shown in NR organ cultures, seems crucial for obtaining human bmMSC secretome with neuroprotective properties.

In summary, this study confirmed the neuroprotective effect of human bmMSC secretome over in vitro retinal neurodegeneration and suggested that the neuroprotective effect of bmMSC secretome in the presence and absence of MSC looks similar. In addition, the neuroprotective properties of the human bmMSC secretome may be associated with activation of the retinal antioxidant machinery, modulation of autophagy, and finally, inhibition of apoptosis and necroptosis. These results agree with those reported previously by our group[11,12] and reinforce the idea that human bmMSC secretome may be a therapeutic strategy for treating RND. The study of the stem cell secretome may be crucial in the development of effective treatments for RND, based on the intravitreal injection of combination of different neuroprotective factors.

Acknowledgments

The authors thank the staff of the Justino Gutierrez S.L. slaughterhouse (Valladolid, Spain) for providing the porcine eye globes used in this work. We also thank Lynda Charters of Medical International (Framingham, MA, USA) for her assistance in this manuscript's final editing and preparation.

Supported by the Spanish Government (PID2019-110709RB-100, RED2018-102417-T, FPU16/04015, PID2020-114585RA-I00 and PID2020-118860RB-I00), Junta de Castilla y León (VA317P18, Infrared2018-UVA06, and GRS1928/A/19), Interred V España Portugal POCTEP (0624_2IQBIONEURO_6_E), and Centro en Red de Medicina Regenerativa y Terapia Celular de Castilla y León. Ricardo Usategui-Martín was funded by the call for postdoctoral contracts UVa2018. Kevin Puertas-Neyra was funded by Fundación Carolina, the call for predoctoral contracts UVa2020 (co-funded by Santander Bank) and predoctoral contracts of the Junta de Castilla y Leon 2021.

Disclosure: **R. Usategui-Martín,** None; **K. Puertas-Neyra,** None; **N. Galindo-Cabello,** None; **L.A. Hernández-Rodríguez,** None; **F. González-Pérez,** None; **J.C. Rodríguez-Cabello,** None; **R. González-Sarmiento,** None; **J.C. Pastor,** None; **I. Fernandez-Bueno,** None

References

1. Gagliardi G, Ben M'Barek K, Goureau O. Photoreceptor cell replacement in macular degeneration and retinitis pigmentosa: A pluripotent stem cell-based approach. *Prog Retin Eye Res*. 2019;71:1–25.
2. Congdon N, O'Colmain B, Klaver CC, et al. Causes and prevalence of visual impairment among adults in the United States. *Arch Ophthalmol*. 2004;122:477–485.
3. Friedman DS, O'Colmain BJ, Munoz B, et al. Prevalence of age-related macular degeneration in the United States. *Arch Ophthalmol*. 2004;122:564–572.
4. Gordois A, Cutler H, Pezzullo L, et al. An estimation of the worldwide economic and health burden of visual impairment. *Global Public Health*. 2012;7:465–481.
5. Cuenca N, Fernández-Sánchez L, Campello L, et al. Cellular responses following retinal injuries and therapeutic approaches for neurodegenerative diseases. *Prog Retin Eye Res*. 2014;43:17–75.
6. Xu H, Chen M, Forrester JV. Para-inflammation in the aging retina. *Prog Retin Eye Res*. 2009;28:348–368.
7. Bhattacharya S, Gangaraju R, Chaum E. Recent Advances in Retinal Stem Cell Therapy. *Curr Mol Biol Rep*. 2017;3:172–182.
8. Tang Z, Zhang Y, Wang Y, et al. Progress of stem/progenitor cell-based therapy for retinal degeneration. *J Transl Med*. 2017;15:99.
9. Labrador-Velandia S, Alonso-Alonso ML, Alvarez-Sanchez S, et al. Mesenchymal stem cell therapy in retinal and optic nerve diseases: an update of clinical trials. *WJSC*. 2016;8:376.
10. Kolomeyer AM, Zarbin MA. Trophic factors in the pathogenesis and therapy for retinal degenerative diseases. *Surv Ophthalmol*. 2014;59:134–165.
11. Labrador-Velandia S, Alonso-Alonso ML, Di Lauro S, et al. Mesenchymal stem cells provide paracrine neuroprotective resources that delay degeneration of co-cultured organotypic neuroretinal cultures. *Exp Eye Res*. 2019;185:107671.
12. Usategui-Martín R, Puertas-Neyra K, García-Gutiérrez MT, Fuentes M, Pastor JC, Fernandez-Bueno I. Human mesenchymal stem cell secretome exhibits a neuroprotective effect over in vitro retinal photoreceptor degeneration. *Mol Ther Methods Clin Dev*. 2020;17:1155–1166.
13. Vizoso FJ, Eiro N, Cid S, Schneider J, Perez-Fernandez R. Mesenchymal stem cell secretome: toward cell-free therapeutic strategies in regenerative medicine. *Int J Mol Sci*. 2017;18.
14. Usategui-Martin R, Fernandez-Bueno I. Neuroprotective therapy for retinal neurodegenerative diseases by stem cell secretome. *Neural Regen Res*. 2021;16:117–118.
15. Labrador Velandia S, Di Lauro S, Alonso-Alonso ML, et al. Biocompatibility of intravitreal injection of human mesenchymal stem cells in immunocompetent rabbits. *Graefes Arch Clin Exp Ophthalmol*. 2018;256:125–134.
16. Fernandez-Bueno I, Usategui-Martin R. Ex vivo model of spontaneous neuroretinal degeneration for evaluating stem cells' paracrine properties. *Methods Mol Biol*. 2021;2269:125–137.
17. Di Lauro S, Rodriguez-Crespo D, Gayoso MJ, et al. A novel co-culture model of porcine central neuroretina explants and retinal pigment epithelium cells. *Mol. Vis*. 2016;22:243–253.
18. Livak KJ, Schmittgen TD. Analysis of relative gene expression data using real-time quantitative PCR and the 2(-Delta Delta C(T)) Method. *Methods*. 2001;25:402–408.
19. Garlipp MA, Nowak KR, Gonzalez-Fernandez F. Cone outer segment extracellular matrix as binding domain for interphotoreceptor retinoid-binding protein. *J Comp Neurol*. 2012;520:756–769.
20. Athanasiou D, Aguilà M, Bevilacqua D, Novoselov SS, Parfitt DA, Cheetham ME. The cell stress machinery and retinal degeneration. *FEBS Lett*. 2013;587:2008–2017.
21. Ruether K, Feigenspan A, Pirngruber J, Leitges M, Baehr W, Strauss O. PKCα is essential for the proper activation and termination of rod bipolar cell response. *Invest Ophthalmol Vis Sci*. 2010;51:6051–6058.
22. Buckingham BP, Inman DM, Lambert W, et al. Progressive ganglion cell degeneration precedes neuronal loss in a mouse model of glaucoma. *J Neurosci*. 2008;28:2735–2744.
23. Vecino E, Rodriguez FD, Ruzafa N, Pereiro X, Sharma SC. Glia-neuron interactions in the mammalian retina. *Prog Retin Eye Res*. 2016;51:1–40.

24. Barber AJ, Lieth E, Khin SA, Antonetti DA, Buchanan AG, Gardner TW. Neural apoptosis in the retina during experimental and human diabetes. Early onset and effect of insulin. *J Clin Invest.* 1998;102:783–791.
25. Kivelä T, Tarkkanen A, Virtanen I. Intermediate filaments in the human retina and retinoblastoma. An immunohistochemical study of vimentin, glial fibrillary acidic protein, and neurofilaments. *Invest Ophthalmol Vis Sci.* 1986;27:1075–1084.
26. Sanges D, Comitato A, Tammaro R, Marigo V. Apoptosis in retinal degeneration involves cross-talk between apoptosis-inducing factor (AIF) and caspase-12 and is blocked by calpain inhibitors. *Proc Natl Acad Sci.* 2006;103:17366–17371.
27. Gavrieli Y, Sherman Y, Ben-Sasson SA. Identification of programmed cell death in situ via specific labeling of nuclear DNA fragmentation. *J Cell Biol.* 1992;119:493–501.
28. Lu C, Li S, Jin M. Activation of the mixed lineage kinase domain like protein-mediated necroptotic pathway in light-induced retinal degeneration. *Invest Ophthalmol Vis Sci.* 2020;61:1287–1287.
29. Klionsky DJ, Abdelmohsen K, Abe A, et al. Guidelines for the use and interpretation of assays for monitoring autophagy (3rd edition). *Autophagy*. 2016;12:1–222.
30. Fernandez-Bueno I, Fernández-Sánchez L, Gayoso MJ, García-Gutierrez MT, Pastor JC, Cuenca N, et al. Time course modifications in organotypic culture of human neuroretina. *Exp Eye Res.* 2012;104:26–38.
31. Bringmann A, Wiedemann P. Müller glial cells in retinal disease. *Ophthalmologica*. 2012;227:1–19.
32. Mollick T, Mohlin C, Johansson K. Human neural progenitor cells decrease photoreceptor degeneration, normalize opsin distribution and support synapse structure in cultured porcine retina. *Brain Res.* 2016;1646:522–534.
33. Jones MK, Lu B, Chen DZ, et al. In vitro and in vivo proteomic comparison of human neural progenitor cell-induced photoreceptor survival. *Proteomics*. 2019;19:e1800213.
34. Nita M, Grzybowski A. The role of the reactive oxygen species and oxidative stress in the pathomechanism of the age-related ocular diseases and other pathologies of the anterior and posterior eye segments in adults. *Oxid Med Cell Longev*. 2016;2016:3164734.
35. B Domènech E, Marfany G. The relevance of oxidative stress in the pathogenesis and therapy of retinal dystrophies. *Antioxidants (Basel)*. 2020;9:347.
36. Whitcup SM, Nussenblatt RB, Lightman SL, Hollander DA. Inflammation in retinal disease. *Int J Inflam*. 2013;2013:724648.
37. Murakami Y, Notomi S, Hisatomi T, et al. Photoreceptor cell death and rescue in retinal detachment and degenerations. *Prog Retin Eye Res.* 2013;37:114–140.
38. Rosenbaum DM, Degterev A, David J, et al. Necroptosis, a novel form of caspase-independent cell death, contributes to neuronal damage in a retinal ischemia-reperfusion injury model. *J Neurosci Res.* 2010;88:1569–1576.
39. Lu J, Holmgren A. The thioredoxin antioxidant system. *Free Radical Biology and Medicine*. 2014;66:75–87.
40. Pannala VR, Dash RK. Mechanistic characterization of the thioredoxin system in the removal of hydrogen peroxide. *Free Radical Biol Med*. 2015;78:42–55.
41. Arnér ESJ. Focus on mammalian thioredoxin reductases — Important selenoproteins with versatile functions. *Biochim Biophys Acta*. 2009;1790:495–526.
42. Holmgren A, Lu J. Thioredoxin and thioredoxin reductase: current research with special reference to human disease. *Biochem Biophys Res Comm*. 2010;396:120–124.
43. Cunningham GM, Roman MG, Flores LC, et al. The paradoxical role of thioredoxin on oxidative stress and aging. *Arch Biochem Biophys*. 2015;576:32–38.
44. Holzerova E, Danhauser K, Haack TB, et al. Human thioredoxin 2 deficiency impairs mitochondrial redox homeostasis and causes early-onset neurodegeneration. *Brain*. 2016;139:346–354.
45. Eleutherio ECA, Silva Magalhães RS, de Araújo Brasil A, Neto MJR, de Holanda Paranhos L. SOD1, more than just an antioxidant. *Arch Biochem Biophys*. 2021;697:108701.
46. Kannan K, Jain SK. Oxidative stress and apoptosis. *Pathophysiology*. 2000;7:153–163.
47. Singh R, Letai A, Sarosiek K. Regulation of apoptosis in health and disease: the balancing act of BCL-2 family proteins. *Nat Rev Mol Cell Biol*. 2019;20:175–193.
48. Pop C, Salvesen GS. Human caspases: activation, specificity, and regulation. *J Biol Chem*. 2009;284:21777–21781.
49. Viringipurampeer IA, Shan X, Gregory-Evans K, Zhang JP, Mohammadi Z, Gregory-Evans CY. Rip3 knockdown rescues photoreceptor cell death in blind pde6c zebrafish. *Cell Death Differ*. 2014;21:665–675.
50. Dong K, Sun X. Targeting death receptor induced apoptosis and necroptosis: a novel therapeutic strategy to prevent neuronal damage in retinal detachment. *Med Hypotheses*. 2011;77:144–146.
51. Trichonas G, Murakami Y, Thanos A, et al. Receptor interacting protein kinases mediate retinal detachment-induced photoreceptor necrosis and compensate for inhibition of apoptosis. *Proc Natl Acad Sci U S A*. 2010;107:21695–21700.
52. Moreno M-L, Mérida S, Bosch-Morell F, Miranda M, Villar VM. Autophagy dysfunction and oxidative stress, two related mechanisms implicated in retinitis pigmentosa. *Front Physiol*. 2018;9.
53. Pyo JO, Nah J, Jung YK. Molecules and their functions in autophagy. *Exp Mol Med*. 2012;44:73–80.
54. Levine B, Kroemer G. Autophagy in the pathogenesis of disease. *Cell*. 2008;132:27–42.
55. Rubinsztein DC, Shpilka T, Elazar Z. Mechanisms of autophagosome biogenesis. *Curr Biol*. 2012;22:R29–34.
56. Behrends C, Sowa ME, Gygi SP, Harper JW. Network organization of the human autophagy system. *Nature*. 2010;466:68–76.
57. Pankiv S, Clausen TH, Lamark T, et al. p62/SQSTM1 binds directly to Atg8/LC3 to facilitate degradation of ubiquitinated protein aggregates by autophagy. *J Biol Chem*. 2007;282:24131–24145.
58. Pivtoraiko VN, Stone SL, Roth KA, Shacka JJ. Oxidative stress and autophagy in the regulation of lysosome-dependent neuron death. *Antioxid Redox Signal*. 2009;11:481–496.
59. Faghiri Z, Bazan NG. PI3K/Akt and mTOR/p70S6K pathways mediate neuroprotectin D1-induced retinal pigment epithelial cell survival during oxidative stress-induced apoptosis. *Exp Eye Res*. 2010;90:718–725.
60. Alonso-Alonso ML, Srivastava GK, Usategui-Martín R, García-Gutierrez MT, Pastor JC, Fernandez-Bueno I. Mesenchymal stem cell secretome enhancement by nicotinamide and vasoactive intestinal peptide: a new therapeutic approach for retinal degenerative diseases. *Stem Cells Int*. 2020;2020:9463548.